DOI: 10.1002/ejic.201100227

Solvothermal Synthesis and Structural Characterisation of Metal-Organic Frameworks with Paddle-Wheel Zinc Carboxylate Clusters and Mixed Ligands

Jia Li,[a] Yu Peng,[a] Hongwei Liang,[a] Yang Yu,[a] Bingjing Xin,[a] Guanghua Li,*[a] Zhan Shi,*[a] and Shouhua Feng[a]

Keywords: Metal-organic frameworks / Zinc / Mixed ligands / Interpenetration / Topology / Paddle-wheel cluster

A series of 3D interpenetrating metal-organic frameworks, namely, $[Zn_3(BPDC)_3(4\text{-}BPT)_{1.5}]\cdot 1.5DMF$ [**1**, BPDC = biphenyl-4,4′-dicarboxylic acid, 4-BPT = 4-amino-3,5-bis(4-pyridyl)-1,2,4-triazole, DMF = dimethylformamide], $[Zn_3(BPDC)_3(4\text{-}PYTZ)_{1.5}]\cdot 1.5DMF$ [**2**, 4-PYTZ = 3,6-bis(pyridin-4-yl)-1,2,4,5-tetrazine], $[Zn_2(OBA)_2(4\text{-}PYTZ)]\cdot 2DMF$ [**3**, OBA = 4,4′-oxybis(benzoate)], $[Zn_2(OBA)_2(3\text{-}PYTZ)\cdot Zn_2(OBA)_2(DMF)_2]\cdot 7DMF$ [**4**, 3-PYTZ = 3,6-bis(pyridin-3-yl)-1,2,4,5-tetrazine] and $[Zn_2(OBA)_2(3\text{-}BPT)]\cdot 2.5DMF$ [**5**, 3-BPT = 4-amino-3,5-bis(3-pyridyl)-1,2,4-triazole] were synthesized by the reaction of $Zn(NO_3)_2\cdot 6H_2O$ with various dipyridyl derivatives and rigid or nonrigid aromatic dicarboxylate ligands. These five compounds were constructed by paddle-wheel-type coordination of Zn^{II} pairs and mixed ligands, which can be simplified as nodes and linkers to generate a variety of topologies. Compounds **1** and **2** exhibit threefold interpenetrated 6-connected **pcu** topology. The interpenetration observed in compounds **1** and **2** is a rare case of heterointerpenetration. The structure of **3** is derived from a 2D double interpenetrated rhombic grid substructure, and is an interesting example of a self-catenated framework displaying a 6-connected uninodal framework with a point symbol $(4^4.6^{10}.8)$. Compound **4**, which is derived from a crosslinked threefold interpenetrated substructure with **pts** topology, displays a self-catenated 4,6-connected binodal framework with the point symbol $(4^2.6^2.7^2)$ $(4^2.6^8.7.8^4)$. Compound **5** exhibits a self-catenated 6-connected structure with **rob** topology, and with the point symbol $(4^8.6^6.8)$. Compounds **1**–**5** also display varied luminescence properties in the solid state.

Introduction

In the past decades research interest in the assembly of metal-organic frameworks (MOFs) has been expanding rapidly due to the construction of intriguing topological architectures[1] and their applications in the fields of luminescence,[2] catalysis,[3] gas absorption[4] and magnetism.[5] Major applications of MOFs are highly dependent on their structural characteristics, especially porosity. The sizes and shapes of the pores within MOFs can be tuned by making use of framework interpenetration,[4a,6] self-catenation,[6,7] supramolecular isomerism[8] or interweaving. Recently, particular attention has been devoted to interpenetration, because the control and tuning of small pore/window sizes within MOFs is crucial for rendering the materials highly functional for specialized applications such as gas storage and the separation of small gas molecules.[9]

It is well known that the structures of MOFs can be determined by the coordination geometry of the metal ions and the structural characteristics of the organic ligands, which means that the topology and interpenetration of MOFs can be controlled and modified by the selection of suitable organic ligands. Usually, long chain ligands can lead to large voids through which independent frameworks can pass, leaving small but well defined voids. Therefore, such ligands are regarded as excellent candidates for the construction of interpenetrating structures.[10] Further, flexible organic ligands can be used to assemble interesting interpenetrating frameworks, thanks to their varied geometries.

The OBA ligand is a typical example of a long, V-shaped, flexible ligand that has been used to promote the formation of interpenetrating and self-catenated frameworks. In our attempt to investigate the interpenetration of MOFs, we chose mixed long chain ligands such as rigid and nonrigid aromatic dicarboxylate and dipyridyl bridging ligands for preparing our MOFs, since different ligand bite angle, length, and the relative orientation of the donor atoms will ultimately alter the pore size of the products; on the other hand, mixed coordination could facilitate the incorporation of functionality into the MOFs. As for the dipyridyl bridging ligands, some analogous linkers derived from the modification of the traditionally employed 4,4′-bipyridine ligand have been extensively studied in coordination chemistry; examples include the introduction of spacers groups between

[a] State Key Laboratory of Inorganic Synthesis and Preparative Chemistry, College of Chemistry, Jilin University, Changchun 130012, People's Republic of China
Fax: +86-431-85168624
E-mail: zshi@mail.jlu.edu.cn
leegh@jlu.edu.cn

Supporting information for this article is available on the WWW under http://dx.doi.org/10.1002/ejic.201100227.

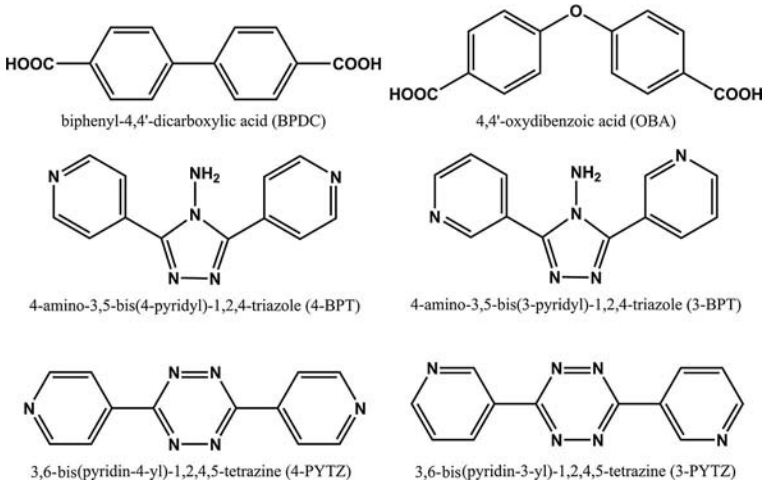

Scheme 1. View of the rigid and nonrigid aromatic dicarboxylate ligands and the long chain dipyridyl bridging ligands used in this work.

the two 4-pyridyl groups, which result in distinct spatial effects that produce unexpected architectures upon metal complexation of the ligand.[2a,4a,5a,8a,11] In our study, we have concentrated on two types of dipyridyl derivatives, one bearing a triazole group and the other a s-tetrazine group. Further, the isomers of the dipyridyl bridging ligands have been used, which differ either in the directionality or in the bent angles of the backbones.

Five new interpenetrated structures, **1**–**5**, containing paddle-wheel $\{Zn_2(COO)_4\}$ clusters were obtained by the simultaneous use in their synthesis of long chain dipyridyl bridging ligands and rigid or nonrigid V-shaped aromatic dicarboxylate ligands that have bridging ability (Scheme 1). The solid-state properties of these crystalline materials, such as their thermal stabilities and fluorescent emissions, have been investigated.

Results and Discussion

Structure of $[Zn_3(BPDC)_3(4\text{-}BPT)_{1.5}]\cdot 1.5DMF$ (1) and $[Zn_3(BPDC)_3(4\text{-}PYTZ)_{1.5}]\cdot 1.5DMF$ (2)

Structural analysis reveals that compound **1** is a 3D triple interpenetrated framework consisting of paddle-wheel $\{Zn_2(COO)_4\}$ clusters and mixed ligands. As shown in Figure 1 (a), the Zn^{II} ion is five-coordinate and displays a typical $ZnNO_4$ square-pyramidal coordination geometry. Each Zn^{II} ion bonds to one nitrogen donor atom from one BPT ligand [Zn(1)–N(5) 2.045(3) Å] in the apical position, and four carboxylate oxygen donor atoms from four BPDC ligands [Zn(1)–O(1) 2.051(3) Å, Zn(1)–O(3) 2.022(3) Å, Zn(1)–O(5) 2.057(3) Å, Zn(1)–O(7) 2.047(3) Å] in the basal plane. Two zinc ions are bridged by four carboxylate groups to form the paddle-wheel dinuclear zinc carboxylate clusters $\{Zn_2(COO)_4\}$ with a Zn–Zn distances of 2.979 Å. The $\{Zn_2(COO)_4\}$ clusters are further linked to four equivalent neighbours through four BPDC ligands to create 2D sheet structures. These 2D sheets are linked in the third dimension by linear dipyridyl ligands, whose nitrogen atoms occupy the axial sites of the $\{Zn_2(COO)_4\}$ clusters, to form a 3D pillared framework (Figure 1, b).

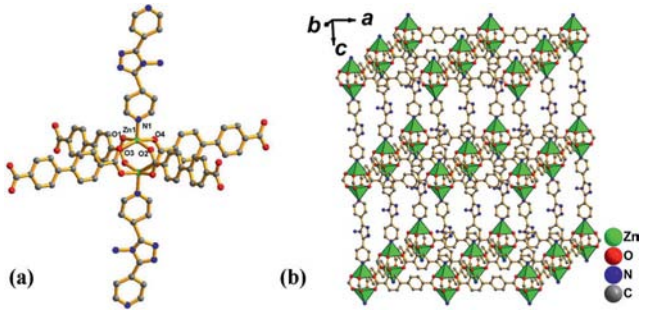

Figure 1. (a) Coordination environment of Zn in **1**; (b) one of the three independent **pcu** nets of **1** (color code, green: zinc, green; gray: carbon, blue: nitrogen, red: oxygen). The lattice DMF molecules are omitted for clarity.

A better insight into the nature of **1** and **2** can be achieved through a topological approach, in particular by reducing the multidimensional structures to simple node and linker nets. In compound **1**, the $\{Zn_2(COO)_4\}$ cluster is surrounded by four bridging BPDC ligands and two linear 4-BPT ligands, which define a six-connected node. Each $\{Zn_2(COO)_4\}$ cluster is further linked to six neighbouring clusters via two types of organic linkers, resulting in a 6-connected threefold interpenetrated structure with **pcu** topology (Figure 2, b). The interpenetration observed for compounds **1** and **2** is a rare case of heterointerpenetration (2+1), they are examples of threefold **pcu** structures with two nets (the red and green nets in Figure 2, a) related by an inversion center and the third net (the blue net in Figure 2, a) being symmetry independent. A similar example has been observed in $Cd(bix)_3(ClO_4)_3$.[6e,12] Although the three interpenetrated frameworks in **1** reduce the pore size, the interpenetration still leaves voids in the structure that are occupied by DMF molecules.

Similar to compound **1**, the structure of compound **2** is also a 3D triple interpenetrated framework with **pcu** topology (Figure 2, b), the interpenetration of compound **2** is

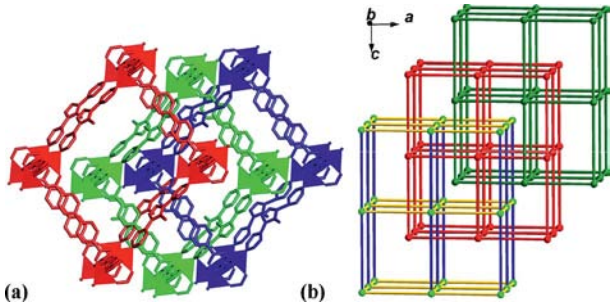

Figure 2. (a) The three independent interpenetrating networks in **1**; (b) A schematic view of the threefold interpenetrated structure of **1** with **pcu** topology.

also heterointerpenetration (Figure 3, c), but 4-PYTZ is present instead of 4-BPT. As shown in Figure 3 (a), the Zn ion is bound by one N atom of a PYTZ ligand (Zn1–N1 2.028 Å) and four O atoms from four individual BPDC ligands [Zn(1)–O(4) 2.053(3) Å, Zn(1)–O(2) 2.035(3) Å, Zn(1)–O(1) 2.026(3) Å, Zn(1)–O(3) 2.064(3) Å] in a square-pyramidal coordination geometry.

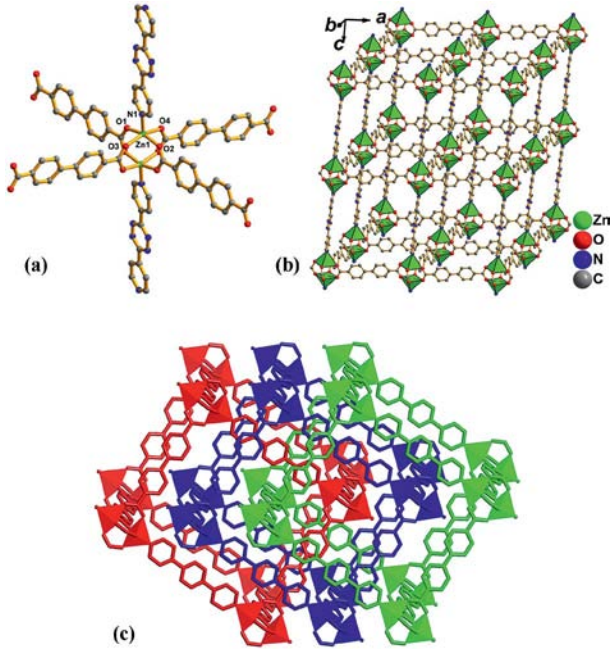

Figure 3. (a) Coordination environment of Zn in **2**; (b)one of the three independent **pcu** nets of **2** ((color code, green: zinc; gray: carbon, blue: nitrogen, red: oxygen). The lattice DMF molecules are omitted for clarity; (c) the three independent interpenetrating networks of **2**.

The average Zn–N distance in compound **2** (2.0373 Å) is appreciably shorter than that in compound **1** (2.0433 Å), and the Zn···Zn separation is smaller than that in **1**. The two compounds also differ in the type of pillar ligand present [4-BPT (in **1**) and 4-PYTZ (in **2**)]. The length of 4-PYTZ (18.0336 Å) is longer than that of 4-BPT (17.583 Å). As a result of this difference in ligand length, the shapes of the 2D sheets that are generated from the $\{Zn_2(COO)_4\}$ clusters and BPDC ligands are different in the two compounds, with the side length and diagonal measurement being 15.213 Å and 23.025 × 19.050 Å for compound **2**, and 15.2129 Å and 22.0026 × 21.1104 Å for compound **1**. Furthermore, the neighbouring layers are staggered with respect to each other, and the distance between two layers is 17.8767 Å in compound **2**, which is longer than that in compound **1** (17.3498 Å).

Structure of $[Zn_2(OBA)_2(4\text{-PYTZ})]\cdot 2DMF$ (3)

Unlike the predictable structures constructed from rigid organic ligands, structures containing flexible organic ligands may display unexpected architectures and topologies, especially interpenetration and self-catenation. In light of this, we replaced the rigid aromatic dicarboxylate ligand (BPDC) with a flexible ligand (OBA), and obtained compound **3**. Structural analysis of compound **3** reveals a 3D coordination framework, which contains paddle-wheel $\{Zn_2(COO)_4\}$ clusters and mixed ligands (OBA and 4-PYTZ) (Figure 4, a). The $\{Zn_2(COO)_4\}$ paddle wheel is further linked to four equivalent neighbours through four OBA anions to give a distorted 2D rhombic grid, with a side length of 10.366 Å and a diagonal measurement of 23.999 × 15.065 Å as defined by the metal–metal distances. Due to the flexibility of the OBA ligand, the –O– spacer between two benzoate groups exhibits a twisted configuration suitable for linking the paddle wheel $\{Zn_2(COO)_4\}$ clusters. Unlike the 2D sheets of compounds **1** and **2**, the 2D rhombic grid of **3** is a distorted to give a wavy layer. Two such layers interpenetrate each other easily, with the paddle-wheel cluster of one layer located at the centre of the channels of the second layer, thus occupying the void of the rhombic grid and producing an infinite 2D double-layer structure (Figure 4, b). As a consequence of this packing arrangement, the framework possesses two kinds of helical chains, and the right-handed and left-handed helical chains alternate in sharing the paddle wheel $\{Zn_2(COO)_4\}$ clusters. These alternating helices are further linked by Zn1–N coordination bonds to afford a 3D framework. As shown in part c of Figure 4, the double helical chains wrap around the axes formed by the organic ligands of the framework, in this manner these attractive structural features are linked together. These infinite helical chains are extended along the crystallographic *b* axis, and the central axis of each helical chain is a twofold screw axis.

The length of the repeating parts of a single helical chain is 15.065 Å, the distance between the repeating parts of each neighbouring helical chain is 7.532 Å and the size of the helical channels is 8.430 × 9.406 Å. The chiral double-layers extend parallel to the *bc* plane and are stacked along the *a* axis. Adjacent double-layers are linked by linear 4-PYTZ ligands to afford a 3D pillared coordination network. The voids between adjacent chiral double-layers are filled with DMF solvent (Figure 4, d). The overall structure of **3** can be described as a 3D framework consisting of Zn-OBA layers and 4-PYTZ pillars. To fully understand such

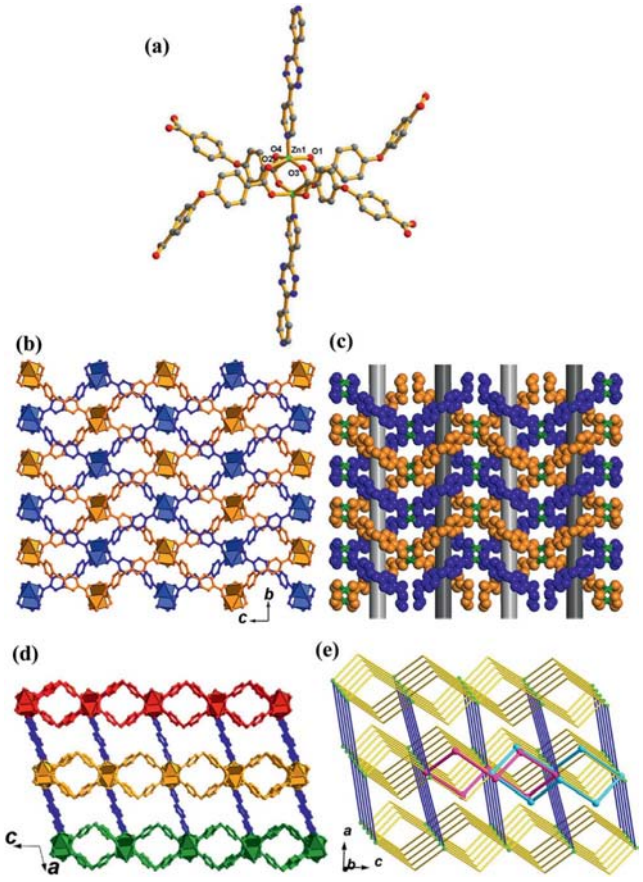

Figure 4. (a) Coordination environment of Zn in **3**. The lattice DMF molecules are omitted for clarity; (b) perspective view of the 3D coordination framework. The large voids between two adjacent chiral double-layers are filled by DMF solvent molecules; (c) view of the double-layer structure (4-BPT molecules have been omitted for clarity); (d) a space-filling plot of the double-stranded helices (the organic molecules have been differentiated by colour for better representation); (e) A schematic view of the 6-c uninodal net with the point symbol ($4^4.6^{10}.8$). The eight-membered rings are emphasized in red, and blue linkers are catenated in the self-catenated network.

a 3D MOF, the $\{Zn_2(COO)_4\}$ cluster can be simplified as 6-connected nodes. Consequently, according to the TOPOS calculations,[13] compound **3** can be reduced to a 6-connected uninodal net with the point symbol ($4^4.6^{10}.8$) (Figure 4, e). An interesting feature of this topology is the presence of self-catenation. In other words, in a similar fashion to molecular knots, rods penetrate the smallest circuits of the same network. As highlighted in Figure 4 (e), two smallest eight-membered circuits that serve to join together the (4,4) nets, form the catenane-like interlocking structure. The self-catenated feature in this structure may be generated from the linking of twofold interpenetrated rhombic grids.

Compared to compound **2**, the overall structure of compound **3** shows no interpenetration, for two possible reasons. First of all, two rhombic layers interpenetrate each other to occupy the layer "void" space, so there is insufficient void space to accept other molecules; secondly, the void between two adjacent double-layers is smaller in **3** than in compound **2**, and can only be filled by solvent molecules.

Structure of $[Zn_2(OBA)_2(3\text{-PYTZ})\cdot Zn_2(OBA)_2(DMF)_2]\cdot 7DMF$ (4)

To explore the effect of ligand isomerism on the structure, the bent dipyridyl ligand 3-PYTZ was used instead of the linear dipyridyls ligand 4-PYTZ; these ligands have the same bridge part but different coordination characteristics. As shown in Figure 5 (a), the geometries of the Zn^{II} ions in compound **4** are square pyramidal. Each Zn1 ion is coordinated to one oxygen atom of DMF and four carboxylate oxygen donor atoms from four OBA ligands, and exhibits a ZnO_5 square coordination geometry with atom O(22) in the apical position [Zn(1)–O(22) 2.007(3) Å], and atoms O(1), O(6), O(11), and O(16) in the basal plane [Zn(1)–O(1) 2.074(3) Å, Zn(1)–O(6) 1.984(3) Å, Zn(1)–O(11) 2.098(3) Å, Zn(1)–O(16) 1.999(3) Å]. Each Zn3 ion is surrounded by one nitrogen donor atom from a 3-PYTZ ligand in the apical position [Zn(3)–N(3) 2.046(3) Å], and four carboxylate oxygen donor atoms from four OBA ligands in the basal plane [Zn(3)–O(4) 2.068(3) Å, Zn(3)–O(10) 2.019(3) Å, Zn(3)–O(19) 2.046(3) Å, Zn(3)–O(15) 2.034(3) Å], revealing a $ZnNO_4$ square-pyramidal coordination geometry. Two adjacent zinc ions are bridged by four carboxylate ligands to form $\{Zn_2(COO)_4\}$ clusters. The $\{Zn_2(COO)_4\}$ clusters have distinct characteristics, the axial positions are occupied by labile solvent ligands or 3-PYTZ ligands, resulting in a square $\{Zn_2(COO)_4\}$ cluster or a trigonal bipyramidal $\{Zn_2(COO)_4N_2\}$ cluster that can be simplified as 4- and 6-connected nodes, respectively.

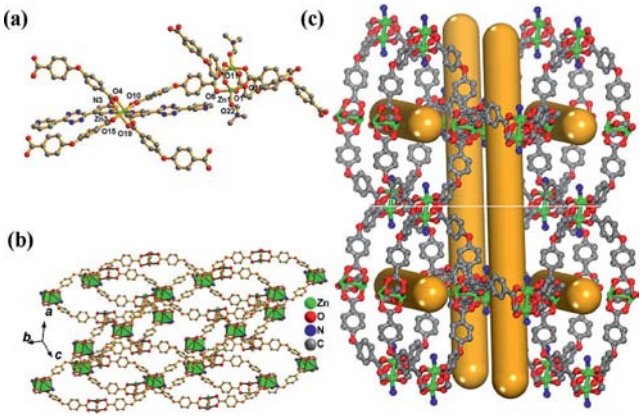

Figure 5. (a) Coordination environment of Zn in **4**. The lattice DMF molecules are omitted for clarity; (b and c) ball-and-stick view of the structure of one of the three independent **pts** frameworks of **4**. 3-PYTZ molecules have been omitted for clarity.

The overall structure of **4** can be described as a very complicated 3D MOF with $\{Zn_2(COO)_4\}$ clusters connecting two types of organic linkers: OBA and 3-PYTZ ligands. To fully understand such a 3D framework, the topological method is used to simplify the structure. Topologically, by considering each $\{Zn_2(COO)_4\}$ cluster as a network node, the overall 3D framework can be rationalized as a new 4,6-connected binodal framework with the point symbol ($4^2.6^2.7^2$) ($4^2.6^8.7.8^4$).

Further analysis of this structure indicates that it consists of three interpenetrated frameworks with **pts** topology (see parts b and c of Figure 5 and Figure 6, a) and $\{Zn_2(COO)_4\}$ cluster nodes and OBA connectors. These frameworks are interconnected by 3-PYTZ spacers (Figure 6, b). This topology indicates the presence of self-catenation. As highlighted in Figure 6 (e), two of the smallest eight-membered circuits form a catenane-like interlocking structure.

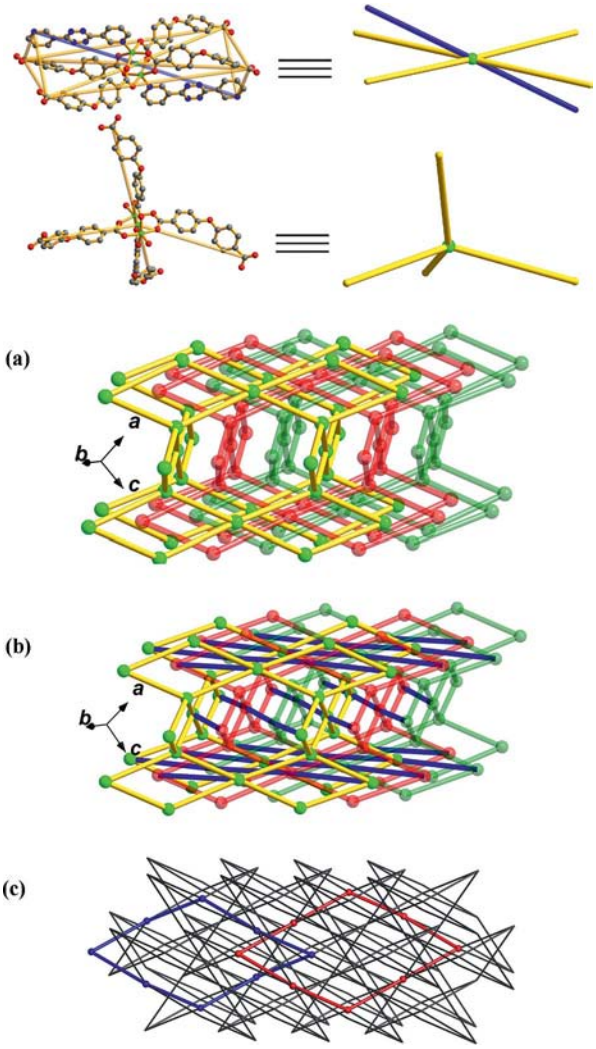

Figure 6. (a) The **pts** topology of the threefold interpenetrated network of a (4,4)-connected ($4^2.8^4$) structure in **4**.3-PYTZ molecules have been omitted for clarity; (b) Topology of the new 4,6- connected framework in **4** with the point symbol ($4^2.6^2.7^2$) ($4^2.6^8.7.8^4$). The square $\{Zn_2(COO)_4\}$ clusters and trigonal-bipyramidal $\{Zn_2(COO)_4N_2\}$ clusters are represented as 4-connected and 6-connected nodes, respectively; (c) The self-catenated network of **4**, the eight-membered rings are printed in red and blue.

Structure of $[Zn_2(OBA)_2(3\text{-BPT})]\cdot 2.5DMF$ (5)

Due to the different orientation of the *N*,*N*′-dipyridyl group donor atoms, 3-BPT exhibits different coordination characteristics than 4-BPT. With this consideration, we used the 3-BPT ligand to construct compound **5**, which is a 3D metal-organic framework. As shown in Figure 7 (a), each Zn^{II} ion bonds to one nitrogen donor atom from one 3-BPT ligand [Zn(1)–N(1) 2.025(3) Å], which is in the apical position, and four carboxylate oxygen donor atoms from four OBA ligands situated in the basal plane [Zn(1)–O(4) 2.030(3) Å, Zn(1)–O(2) 2.043(3) Å, Zn(1)–O(1) 2.058(3) Å, Zn(1)–O(3) 2.067(3) Å]. Therefore the Zn^{II} ions exhibit $ZnNO_4$ square-pyramidal coordination geometry. The distance between the two zinc ions of the $\{Zn_2(COO)_4\}$ cluster is 2.932(8) Å. Similar to **3**, the overall structure of **5** can also be described as a 3D framework comprising Zn-OBA layers and 3-BPT spacers. Each $\{Zn_2(COO)_4\}$ cluster is connected to six other clusters through four OBA ligands and two 3-BPT ligands to generate a neutral six-connected 3D network.

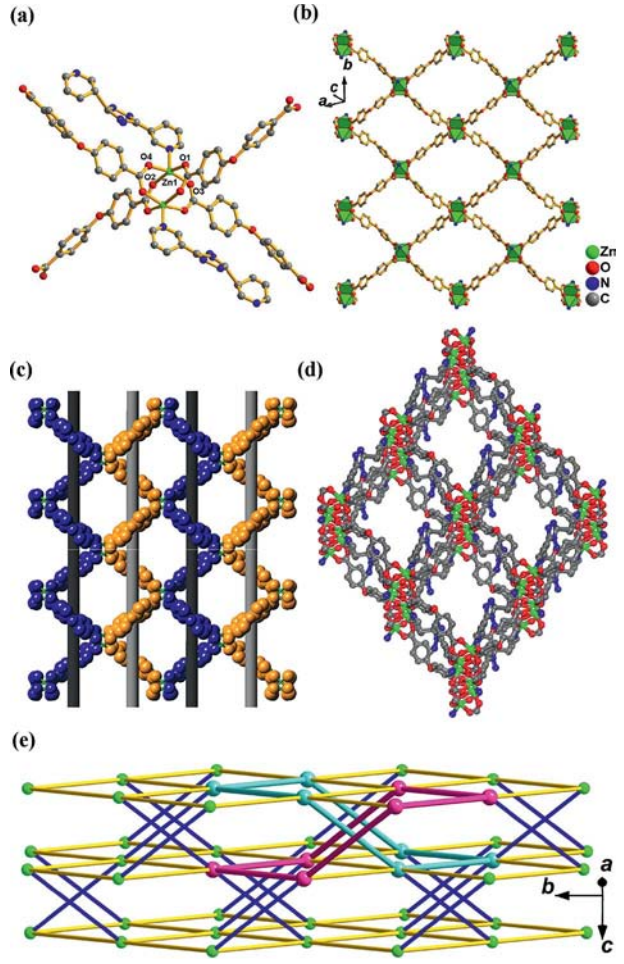

Figure 7. (a) Coordination environment of Zn in **5**. The lattice DMF molecules are omitted for clarity; (b) view of the structure of one layer in the structure of **5**. The 3-BPT molecules have been omitted for clarity; (c) view of the space-filling plot of one layer in the structure of **5**, in which the organic molecules have been differentiated by colours for better representation; (d) a 1D rectangular channel in **5** as viewed along the *c*-axis; (e) a schematic view of a 6-c uninodal **rob** net with the point symbol ($4^8.6^6.8$). The six-membered rings within the self-catenated network are emphasized in red and blue.

In compound **5** the two pyridyl nitrogen atoms of 3-BPT are in a *trans*-conformation. In the Zn-OBA layer of **5** (see parts b and c of Figure 7), the $\{Zn_2(COO)_4\}$ clusters are bridged by OBA ligands to form helical chains with a pitch of 18 Å along the *b* axis. The helical chains have opposite handedness and adjacent chains are interconnected by $\{Zn_2(COO)_4\}$ clusters. When the structure of **5** is viewed along the *c* axis, rhombic channels, which are occupied by solvent molecules, are observed (Figure 7, d). From the viewpoint of network topology, the overall 3D structure of **5** can be rationalized as a uninodal 6-connected framework with **rob** topology [point symbol $(4^8.6^6.8)$], in which the $\{Zn_2(COO)_4\}$ clusters act as network nodes and the two types of organic ligands, OBA (red) and 3-BPT (blue), as linkers (Figure 7, e). One key feature of this topology is the cross-linking of 2D (4,4) nets by parallel rods. The 2D sheets of $\{Zn_2(COO)_4\}$ clusters are bridged by bidentate OBA ligands and 3-BPT pillars which are crisscrossed to bridge at two different angles relative to the sheets. Another interesting feature of this topology is the presence of self-catenation. As highlighted in Figure 7 (e), two of the smallest six-membered circuits that serve to join together the (4,4) nets form a catenane-like interlocking structure.[14] Each six-membered circuit with a link within a layer is catenated by two interlayer rods, and the six-membered circuits mutually interweave to form a self-catenated structural motif.

Thermal Stability

The thermal stabilities of the compounds were investigated by thermogravimetric (TG) analysis (see Figure S1 in the Supporting Information). Compound **1** loses its lattice DMF molecules at 79–136 °C (calcd. 7.93% and found 7.94%). The final residual weight for **1** corresponds to that of ZnO (JCPDS: 74–0534) (calcd. 17.50% and found 17.65%). The TG curve for compound **2** show a weight loss corresponding to the lattice DMF molecules over the 68–145 °C range (calcd. 7.94% and found 7.51%), after which the weight loss is accelerated, and finally ZnO is yielded. The first weight loss for compound **3** occurs from 112 to 220 °C and corresponds to the elimination of two DMF molecules from the structure (calcd. 14.26% and found 16.43%). The final residual weight for **3** corresponds to that of ZnO. For compound **4**, the first weight loss occurs from 98 to 325 °C and can be ascribed to the departure from the structure of coordinated DMF molecules and lattice DMF molecules (calcd. 30.18% and found 29.46%). The final residual weight for **4** corresponds to that of ZnO. The TG curve for **5** shows that a weight loss of 17.32% occurs in 86–157 °C range, and is presumably due to the removal from the structure of two and a half lattice DMF molecules (calcd. 17.18%). The final residual weight for **5** corresponds to that of ZnO.

Photoluminescence Properties

Metal-organic frameworks constructed from d^{10} metal centers and conjugated organic ligands are promising candidates for hybrid photoactive materials with potential application as light emitting diodes (LEDs). These crystalline solids usually display controllable photoluminescence properties and high thermal stability. Thus, the room temperature solid-state emission spectra of the as-synthesized Zn^{II} compounds **1**–**5** have been investigated. As reported previously, solid H_2OBA and H_2BPDC ligands are nearly non-fluorescent in the 400–800 nm range after excitation at room temperature with light with wavelengths between 360 and 450 nm.[15] To further analyze the nature of these emission bands, the photoluminescence properties of the ligands 4-BPT, 3-BPT, 4-PYTZ and 3-PYTZ have also been explored (see Figure S2a in the Supporting Information). When excited with 320 nm light, emission peaks occur in the emission spectra at 406/464 nm (for **1**), 414/458 nm (for **2**), 440/470 nm (for **3**), 406/462 nm (for **4**) and 382/480 nm (for **5**) (see Figure S2b in the Supporting Information). The free 4-BPT and 3-BPT ligands contain pyridyl and triazole conjugated groups, and they show two weak emission peaks in their spectra at 382/476 and 382/490 nm (λ_{ex} = 320 nm), respectively. The free 4-PYTZ and 3-PYTZ ligands contain pyridyl and tetrazine conjugated groups, and they show two weak emission peaks in their spectra at 428/460 and 410/462 nm (λ_{ex} = 320 nm), respectively (see Figure S2a in the Supporting Information). In comparison the free N-donor ligands, the emissions of compounds **1**–**5** are noticably shifted. The Zn^{II} ion with d^{10} configuration is difficult to oxidize or reduce. Thus, it can be presumed that the peaks appearing at 462 nm in the spectrum of **4** and at 382 nm in the spectrum of **5** can be assigned to the intraligand $\pi \rightarrow \pi^*$ transitions of the 3-PYTZ and 3-BPT ligands, respectively. The other fluorescence peaks appearing at around 400 and 460 nm in the spectra of **1**–**5** may be ascribed to ligand-centred transitions, and the small red or blue shifts of these peaks compared with those of the free ligands is a result of metal-ligand coordination interactions. Furthermore, the considerable enhancement of the intensity of these peakss relative to those observed in the ligand spectra may be attributed to the increased rigidity of the ligands when they are bound to the metal centre, which effectively reduces the energy loss. These results indicate that such metal compounds may be good candidates as potential photoactive materials.

Conclusions

In summary, a series of self-assembled metal-organic frameworks have been constructed with long-chain ligands bearing a triazole or s-tetrazian groups, rigid or nonrigid aromatic dicarboxylate ligands, and zinc salts. These frameworks illustrate once more the aesthetic diversity of coordination chemistry. The results from this study reveal that paddle-wheel $\{Zn_2(COO)_4\}$ clusters can be constructed by changing the aromatic dicarboxylate ligands coordinated to the Zn ions. Furthermore, as a result of the participation of different pyridyl bridging ligands that act as secondary ligands, compounds **1**–**5** with intriguing topologies have

been synthesized. Herein, the design and assembly of MOFs with charming topologies can be attributed to the proper selection of carboxylic acid ligands as well as various pyridyl bridging ligands. Further systematic work with the aim of studying the effects of the structural features of other metal ions, such as Co, Cd, and Mn, on the architecture of the resulting frameworks is now in progress in our laboratory.

Experimental Section

Materials and Physical Measurements: With the exception of the ligands of 3-BPT, 4-BPT, 3-PYTZ and 4-PYTZ, which were synthesized according to a literature procedure,[16] all reagents and solvents for syntheses were commercially available and used as received without further purification. Elemental analyses were performed on a Perkin–Elmer 2400 element analyzer. The FTIR spectra were collected on a Nicolet Impact 410 FTIR spectrometer. Thermogravimetric experiments were performed with a TGA Q500 V20.10 Build 36; data were collected from room temperature to 800 °C at a heating rate of 10 °C/min. The emission and excitation spectra of the samples were recorded on an Edinburgh Instruments FLS920 spectrofluorimeter equipped with both continuous (450 W) and pulsed xenon lamps. X-ray powder diffraction (XRPD) patterns were recorded on a Rigaku D/max 2550 X-ray Powder Diffractometer, at a speed of 1°/min. The calculated XRPD patterns were produced from single-crystal X-ray diffraction data.

Syntheses: The five coordination polymers were all synthesized under solvothermal conditions. In each synthetic procedure an approximate metal/dipyridyl ligand/dicarboxylate ligand starting composition of 1:1:1 was utilized.

Synthesis of Compound 1: A mixture of $Zn(NO_3)_2{\cdot}6H_2O$ (0.0297 g, 0.1 mmol), H_2BPDC (0.0242 g, 0.1 mmol), and 4-BPT (0.024 g, 0.1 mmol) was suspended in a solvent mix containing DMF (2.5 mL) and acetonitrile (2.5 mL). The mixture was heated in a Teflon®-lined steel bomb at 80 °C for 24 h. Colourless block-shaped crystals formed were collected in 57% yield (based on Zn). $C_{64.5}H_{54.5}N_{10.5}O_{13.5}Zn_3$ (1388.80): calcd. C 55.97, H 2.78, N 7.56; found C 55.92, H 3.98, N 7.53. IR (KBr): $\tilde{\nu}$ = 3311 (w), 2927 (w), 1957 (w), 1674 (s), 1398 (s), 1093 (s), 841 (m), 771 (s), 679 (m), 453 (m) cm^{-1}.

Synthesis of Compound 2: The same synthetic procedure reported for **1** was used to prepare **2**, except that 4-PYTZ was replaced by 4-BPT, and acetonitrile was replaced by EtOH. Red prism crystals of **2** were collected in 70% yield (based on Zn). $C_{64.5}H_{52.5}N_{10.5}O_{13.5}Zn_3$ (1386.78): calcd. C 55.81, H 3.79, N 10.37; found C 55.84, H 3.77, N 10.54. IR (KBr): $\tilde{\nu}$ = 3060 (w), 2927 (w), 1676 (s), 1639 (m), 1606 (s), 1394 (s), 1089 (w), 841 (m), 769 (m), 603 (m), 455 (w) cm^{-1}.

Synthesis of Compound 3: The same synthetic procedure reported for **2** was used to prepare **3**, except that H_2BPDC was replaced by H_2OBA (0.258 g, 0.1 mmol), to give colourless block-shaped X-ray-quality crystals in 75% yield (based on Zn). $C_{46}H_{38}N_8O_{12}Zn_2$ (1025.58): calcd. C 53.82, H 3.71, N 10.92; found C 53.84, H 3.74, N 10.89. IR (KBr): $\tilde{\nu}$ = 3073 (w), 2922 (w), 1675 (s), 1631 (s), 1594 (m), 1396 (s), 1227 (s), 1159 (m), 1090 (w), 1063 (w), 876 (m), 783 (m), 737 (w), 656 (m), 606 (m), 534 (w), 455 (w) cm^{-1}.

Synthesis of Compound 4: A mixture of $Zn(NO_3)_2{\cdot}6H_2O$ (0.0297 g, 0.1 mmol), H_2OBA (0.0258 g, 0.1 mmol), and 3-PYTZ (0.024 g, 0.1 mmol) was suspended in a solvent mix containing DMF (2.5 mL) and methanol (2.5 mL). This mixture was heated in a Teflon-lined steel bomb at 60 °C for 72 h. Red block-shaped crystals suitable for X-ray diffraction analysis were collected in 35% yield (based on Zn). $C_{95}H_{103}N_{15}O_{29}Zn_4$ (2180.40): calcd. C 52.28, H 4.72, N 9.63; found C 52.31, H 4.75, N 9.60. IR (KBr): $\tilde{\nu}$ = 3074 (w), 2932 (w), 1662 (s), 1631 (s), 1597 (s), 1498 (m), 1394 (s), 1240 (s), 1161 (m), 1097 (w), 1012 (w), 879 (m), 782 (m), 698 (m), 660 (m), 525 (w), 504 (w), 448 (w) cm^{-1}.

Synthesis of Compound 5: The same synthetic procedure reported for **4** was used to prepare **5**, except that 3-PYTZ was replaced by 3-BPT (0.0236 g, 0.1 mmol), to produce red block-shaped crystals of **5** in 69% yield (based on Zn). $C_{47.50}H_{47.50}N_{8.50}O_{12.50}Zn_2$ (1068.18): calcd. C 53.41, H 4.48, N 11.15; found C 53.5, H 4.46, N 11.3. IR (KBr): $\tilde{\nu}$ = 3070 (w), 2935 (w), 1681 (s), 1626 (s), 1595 (s), 1501 (w), 1392 (s), 1307 (w), 1289 (w), 1246 (s), 1157 (s), 1118 (w), 1044 (w), 1007 (w), 879 (w), 781 (m), 698 (m), 669 (w), 513 (w), 451 (w) cm^{-1}.

X-ray Structure Determinations: X-ray single-crystal diffraction data for **1** and **3**–**5** were collected on a Rigaku RAXIS-RAPID

Table 1. Crystallographic data for **1**–**5**.

Compound	**1**	**2**	**3**	**4**	**5**
Molecular formula	$C_{64.50}H_{54.50}N_{10.50}O_{13.50}Zn_3$	$C_{64.50}H_{52.50}N_{10.50}O_{13.50}Zn_3$	$C_{46}H_{38}N_8O_{12}Zn_2$	$C_{95}H_{103}N_{15}O_{29}Zn_4$	$C_{47.50}H_{47.50}N_{8.50}O_{12.50}Zn_2$
Fw	1388.80	1386.78	1025.58	2180.40	1068.18
Crystal system	triclinic	triclinic	monoclinic	monoclinic	monoclinic
Space group	$P\bar{1}$	$P\bar{1}$	$C2/c$	$C2/c$	$C2/c$
a [Å]	15.241(3)	15.224(3)	27.932(6)	25.367(5)	21.891(4)
b [Å]	15.251(3)	15.259(3)	7.5323(15)	16.334(3)	18.090(4)
c [Å]	17.584(4)	18.059(4)	23.999(5)	21.515(4)	17.127(3)
α [°]	80.73(3)	91.84 (3)			
β [°]	88.38(3)	96.69(3)	103.99(3)	97.30(3)	106.62(3)
γ [°]	87.63(3)	98.28(3)			
V [Å^3]	4029.3(14)	4117.8(14)	4899.3(17)	8842(3)	6499(2)
Z	2	2	4	4	4
$D_{calcd.}$ [g/cm^3]	1.145	1.118	1.390	1.638	1.092
$F(000)$	1426	1422	2104	4520	2208
Final R indices	R_1 = 0.0628	R_1 = 0.0580	R_1 = 0.0370	R_1 = 0.0529	R_1 = 0.0704
$[I > 2\sigma(I)]$[a,b]	wR_2 = 0.2068	wR_2 = 0.1225	wR_2 = 0.0913	wR_2 = 0.1386	wR_2 = 0.2046
R indices	R_1 = 0.0863	R_1 = 0.1460	R_1 = 0.0508	R_1 = 0.0841	R_1 = 0.0829
(all data)	wR_2 = 0.2217	wR_2 = 0.1346	wR_2 = 0.0953	wR_2 = 0.1501	wR_2 = 0.2135

[a] $R_1 = ||F_o| - |F_c||/\Sigma|F|_o$. [b] $wR_2 = [\Sigma w(F_o^2 - F_c^2)^2/\Sigma w(F_o^2)^2]^{1/2}$. $w = 1/[\sigma^2(F_o^2) + (ap)^2 + (bp)]$, $p = [\max(F_o^2, 0) + 2(F_c^2)]/3$.

diffractometer. The data processing was accomplished with the PROCESS-AUTO program. XRD data collection and structural analysis of **2** were performed on a Bruker SMART CCD diffractometer equipped with a graphite monochromator. The SMART software was used for data collection, for indexing the reflections, and for determining the unit cell parameters; the collected data were integrated with the SAINT software. All data were collected at of 20 °C. Structure solutions were by direct methods performed with the SHELXL crystallographic software package. All non-hydrogen atoms were easily found in the difference Fourier maps. All non-hydrogen atoms were refined anisotropically. Further crystallographic data and structure refinement details are summarized in Table 1. The 4-BPT ligand in compound **1**, and the 3-BPT ligand in compound **5** are disordered, the models for which are shown in Figures S3 and S4 in the Supporting Information.

CCDC-808319 (for **1**), -808320 (for **2**), -808321 (for **3**), -808322 (for **4**), and -808323 (for **5**) contain the supplementary crystallographic data for this paper. These data can be obtained free of charge from The Cambridge Crystallographic Data Centre via www.ccdc.cam.ac.uk/data_request/cif.

Supporting Information (see footnote on the first page of this article): Thermogravimetric analyses (Figure S1), solid-state fluorescence emission spectra (Figure S2), and disorder models for ligands in compounds **1** and **5** (Figure S3–S4). IR spectra (Figure S5–S9) and powder XRD patterns (Figure S10-S14) for **1**–**5**.

Acknowledgments

This work was supported by the National Natural Science Foundation of China (grant numbers 20971054 and 90922034) and the Key Project of the Chinese Ministry of Education.

[1] a) O. K. Farha, C. D. Malliakas, M. G. Kanatzidis, J. T. Hupp, *J. Am. Chem. Soc.* **2010**, *132*, 950–952; b) G. E. Kostakis, A. K. Powell, *Coord. Chem. Rev.* **2009**, *253*, 2686; c) X. H. Bu, M. L. Tong, H. C. Chang, S. Kitagawa, S. R. Batten, *Angew. Chem. Int. Ed.* **2004**, *43*, 192–195; d) M. O'Keeffe, M. A. Peskov, S. J. Ramsden, O. M. Yaghi, *Acc. Chem. Res.* **2008**, *41*, 1782–1789; e) O. Delgado-Friedrichs, M. O'Keeffe, O. M. Yaghi, *Acta Crystallogr., Sect. A* **2003**, *59*, 22–27.

[2] a) S. I. Vagin, A. K. Ott, S. D. Hoffmann, D. Lanzinger, B. Rieger, *Chem. Eur. J.* **2009**, *15*, 5845–5853; b) V. W. W. Yam, K. K. W. Lo, W. K. M. Fung, C. R. Wang, *Coord. Chem. Rev.* **1998**, *171*, 17–41; c) P. Wang, J. P. Ma, Y. B. Dong, R. Q. Huang, *J. Am. Chem. Soc.* **2007**, *129*, 10620–10621; d) R. Q. Zou, R. Q. Zhong, M. Du, D. S. Pandey, Q. Xu, *Cryst. Growth Des.* **2007**, *8*, 452–459; e) S. Swavey, R. Swavey, *Coord. Chem. Rev.* **2009**, *253*, 2627–2638; f) M. D. Allendorf, C. A. Bauer, R. K. Bhaktaa, R. J. T. Houka, *Acc. Chem. Res.* **2009**, *42*, 1330–1352; g) J. R. Li, Y. Tao, Q. Yu, X. H. Bu, *Chem. Commun.* **2007**, 1527–1529.

[3] a) J. S. Seo, D. Whang, H. Lee, S. I. Jun, J. Oh, Y. J. Jeon, K. Kim, *Nature* **2000**, *404*, 982–986; b) R. Q. Zou, H. Sakurai, S. Han, R. Q. Zhong, Q. Xu, *J. Am. Chem. Soc.* **2007**, *129*, 8402–8403; c) J. Y. Lee, O. K. Farha, J. Roberts, K. A. Scheidt, S. T. Nguyen, J. T. Hupp, *Acc. Chem. Res.* **2009**, *42*, 1450–1459.

[4] a) M. Xue, S. Q. Ma, Z. Jin, R. M. Schaffino, G. S. Zhu, E. B. Lobkovsky, S. L. Qiu, B. L. Chen, *Inorg. Chem.* **2008**, *47*, 6825–6828; b) D. Bradshaw, T. J. Prior, E. J. Cussen, J. B. Claridge, M. J. Rosseinsky, *J. Am. Chem. Soc.* **2004**, *126*, 6106–6114; c) B. Chen, M. Eddaoudi, S. T. Hyde, M. O'Keeffe, O. M. Yaghi, *Science* **2001**, *291*, 1021–1023; d) X. Lin, A. J. Blake, C. Sun, X. Z. Wilson, N. R. Champness, M. W. George, P. Hubberstey, R. Mokaya, M. Schröder, *J. Am. Chem. Soc.* **2006**, *128*, 10745–10753; e) J. L. C. Rowsell, A. R. Millward, K. S. Park, O. M. Yaghi, *J. Am. Chem. Soc.* **2004**, *126*, 5666–5667; f) D. N. Dybstev, H. Chun, K. Kim, *Angew. Chem. Int. Ed.* **2004**, *43*, 5033–5036; g) L. Q. Ma, A. Jin, Z. G. Xie, W. B. Lin, *Angew. Chem. Int. Ed.* **2009**, *48*, 9905–9908; h) J. An, S. J. Geib, N. L. Rosi, *J. Am. Chem. Soc.* **2010**, *132*, 38–39; i) S. M. Zhang, Z. Chang, T. L. Hu, X. H. Bu, *Inorg. Chem.* **2010**, *49*, 11581–11586.

[5] a) W. Wernsdorfer, N. Aliaga-Alcalde, D. N. Hendrickson, G. Christou, *Nature* **2002**, *416*, 406–409; b) S. Konar, P. S. Mukherjee, E. Zangrando, F. Lloret, N. R. Chaudhuri, *Angew. Chem. Int. Ed.* **2002**, *41*, 1561–2563; c) J. R. Li, Q. Yu, Y. Tao, X. H. Bu, J. Ribas, S. R. Batten, *Chem. Commun.* **2007**, 2290–2292.

[6] a) L. Carlucci, G. Ciani, D. M. Proserpio, S. Rizzato, *Chem. Eur. J.* **2002**, *8*, 1519–1526; b) S. R. Batten, R. Robson, *Angew. Chem. Int. Ed.* **1998**, *37*, 1460–1494; c) K. L. Mulfort, O. K. Farha, C. D. Malliakas, M. G. Kanatzidis, J. T. Hupp, *Chem. Eur. J.* **2010**, *16*, 276–281; d) D. F. Sun, S. Q. Ma, Y. X. Ke, D. J. Collins, H. C. Zhou, *J. Am. Chem. Soc.* **2006**, *128*, 3896–3897; e) V. A. Blatov, L. Carlucci, G. Ciani, D. M. Proserpio, *CrystEngComm* **2004**, *6*, 377–395; f) Z. X. Li, Y. Xu, Y. Zuo, L. Li, Q. H. Pan, T. L. Hu, X. H. Bu, *Cryst. Growth Des.* **2009**, *9*, 3904–3909.

[7] a) C. S. Campos-Fernández, B. L. Schottel, H. T. Chifotides, J. K. Bera, J. Bacsa, J. M. Koomen, D. H. Russell, K. R. Dunbar, *J. Am. Chem. Soc.* **2005**, *127*, 12909–12923; b) M. L. Tong, X. M. Chen, S. R. Batten, *J. Am. Chem. Soc.* **2003**, *125*, 16170–16171; c) B. F. Abrahams, M. J. Hardie, B. F. Hoskins, R. Robson, E. E. Sutherland, *J. Chem. Soc., Chem. Commun.* **1994**, 1049–1050.

[8] a) M. Du, X. J. Jiang, X. J. Zhao, *Inorg. Chem.* **2007**, *46*, 3984–3995; b) B. Y. Li, Y. Peng, G. H. Li, J. Hua, Y. Yu, D. Jin, Z. Shi, S. H. Feng, *Cryst. Growth Des.* **2010**, *10*, 2192–2201.

[9] B. Chen, S. C. Xiang, G. D. Qian, *Acc. Chem. Res.* **2010**, *43*, 1115–1134.

[10] a) X. L. Wang, C. Qin, E. B. Wang, Z. M. Su, *Chem. Eur. J.* **2006**, *12*, 2680–2691; b) B. F. Abrahams, S. R. Batten, M. J. Grannas, H. Hamit, B. F. Hoskins, R. Robson, *Angew. Chem. Int. Ed.* **1999**, *38*, 1475–1477; c) X. H. Huang, T. L. Sheng, S. C. Xiang, R. B. Fu, S. M. Hu, Y. M. Li, X. T. Wu, *Inorg. Chem.* **2006**, *45*, 497–500; d) X. L. Wang, C. Qin, E. B. Wang, Y. G. Li, Z. M. Su, L. Xu, L. Carlucci, *Angew. Chem. Int. Ed.* **2005**, *44*, 5824–5827; e) S. R. Batten, A. R. Harris, P. Jensen, K. S. Murray, A. Ziebell, *J. Chem. Soc., Dalton Trans.* **2000**, 3829–3835.

[11] a) M. Du, X. J. Jiang, X. J. Zhao, *Inorg. Chem.* **2006**, *45*, 3998–4006; b) M. Du, Z. H. Zhang, Y. P. You, X. J. Zhao, *CrystEngComm* **2008**, *10*, 306–321; c) O. K. Farha, J. T. Hupp, *Acc. Chem. Res.* **2010**, *43*, 1166–1175; d) M. C. Aragoni, M. Arca, N. R. Champness, M. De Pasquale, F. A. Devillanova, F. Isaia, V. Lippolis, N. S. Oxtoby, C. Wilson, *CrystEngComm* **2005**, *7*, 363–369; e) M. Felloni, A. J. Blake, P. Hubberstey, C. Wilson, M. Schroder, *Cryst. Growth Des.* **2009**, *9*, 4685–4699; f) M. X. Li, H. Wang, S. W. Liang, M. Shao, X. He, Z. X. Wang, S. R. Zhu, *Cryst. Growth Des.* **2009**, *9*, 4626–4633.

[12] V. A. Blatov, *IUCr Comp. Comm. Newsl.* **2006**, *7*, 4–38.

[13] B. F. Abrahams, B. F. Hoskins, R. Robson, D. A. Slizys, *CrystEngComm* **2002**, *4*, 478–482.

[14] J. Zhang, Y. G. Yao, X. H. Bu, *Chem. Mater.* **2007**, *19*, 5083–5089.

[15] J. Tao, J. X. Shi, M. L. Tong, X. X. Zhang, X. M. Chen, *Inorg. Chem.* **2001**, *40*, 6328–6330.

[16] a) F. Bentiss, M. Lagrenée, M. Traisnel, B. Mernari, H. Elattari, *J. Heterocycl. Chem.* **1999**, *36*, 149–152; b) R. Charonnat, P. Fabiani, *R. Hebd. Seances Acad. Sci.* **1955**, *241*, 1783–1785; c) N. S. Oxtoby, A. J. Blake, N. R. Champness, C. Wilson, *CrystEngComm* **2003**, *5*, 82–86.

Received: March 5, 2011
Published Online: May 12, 2011

